Exocytosis of the silicified cell wall of diatoms involves extensive membrane disintegration

Diede de Haan[1], Hadas Peled-Zehavi[1], Yoseph Addadi[2], Oz Ben Joseph[1], Lior Aram[1] and Assaf Gal[1*]

[1]Department of Plant and Environmental Sciences, Weizmann Institute of Science, Rehovot, Israel
[2]Life Science Core Facilities, Weizmann Institute of Science, Rehovot, Israel
*email: assaf.gal@weizmann.ac.il

Keywords

Biomineralization; Diatoms, Exocytosis, Silica deposition vesicle, membrane dynamics

Abstract

Diatoms are unicellular algae that are characterized by their silica cell walls. The silica elements form intracellularly in a membrane-bound organelle, and are exocytosed after completion. How diatoms maintain membrane homeostasis during the exocytosis of these large and rigid silica elements is a long-standing enigma. We studied membrane dynamics during cell wall formation and exocytosis in the diatom *Stephanopyxis turris*, using live-cell confocal microscopy and advanced electron microscopy. Our results provide detailed information on the ultrastructure and dynamics of the silicification process, showing that during cell wall formation, the organelle membranes tightly enclose the mineral phase, creating a precise mold of the delicate geometrical patterns. Surprisingly, during exocytosis of the mature silica elements, the proximal organelle membrane becomes the new plasma membrane, and the distal membranes gradually disintegrate into the extracellular space without any noticeable endocytic retrieval or extracellular repurposing. These observations suggest that diatoms evolved an extraordinary exocytosis mechanism in order to secrete their cell wall elements.

Introduction

Diatoms are important members of marine and freshwater phytoplankton communities[1]. This diverse group of unicellular algae is characterized by silica cell walls with intricate species-specific shapes and patterns[2]. Despite immense morphological diversity between species, most diatom cell walls have the same, conserved layout of two similarly shaped silica 'shells' that partially overlap like a petri-dish. Each 'shell' in itself consists of a valve and a series of girdle bands. The valves usually define the shape of the cell, are richly ornamented, and contain hierarchical pore patterns. The girdle bands form partially overlapping rings that surround the sidewalls of the cells.

Diatom cell wall formation is genetically controlled and under strict biological regulation[3–6]. Silicification is usually an intracellular process, taking place inside a membrane-bound organelle, the silica deposition vesicle (SDV)[7–9]. The chemical environment inside the SDV, and the cellular regulation over its contents and shape, exert tight control over the silicification process, resulting in highly specific and reproducible cell wall architectures[10–14]. After intracellular formation, the mature silica elements are exocytosed to cover the cell surface[7,15]. Such exocytosis events are extraordinary in cell biology since the content of the SDV is an enormous solid structure that needs to be secreted without endangering the integrity of the cell.

In classical exocytosis, an intracellular membrane vesicle fuses with the plasma membrane to deliver its content to the extracellular space. Homeostasis of cell surface area and plasma membrane composition can be maintained through a transient fusion that prevents the secreting vesicle from integrating with the plasma membrane, or by offsetting the added membrane with compensatory endocytosis[16]. However, it is difficult to envision how these mechanisms can be applied to the secretion of diatom cell walls due to their large size and rigidity. In some species, the valve covers as much as half of the total cell surface, causing the surface area of the SDV membrane to be similar to that of the entire plasma membrane. The fusion of such an SDV membrane with the plasma membrane would lead to an almost instantaneous doubling of the membrane surface area. Hence, the mechanism that diatoms use to maintain the needed large-scale membrane homeostasis during cell wall exocytosis is a long-standing enigma.

Early ultrastructural studies brought forward several models for silica cell wall exocytosis in diatoms[15,17–24] (Fig. 1). One scenario suggests that the newly formed valve is externalized through

formation of a new plasma membrane underneath it (Fig. 1 A). The SDV membrane and the original plasma membrane around the new valve remain in place, forming an organic layer around the silica (Fig. 1 B). An alternative is that the valve is externalized as a result of localized fusion of the SDV and plasma membrane at the valve edge, such that the proximal part of the SDV membrane becomes the new plasma membrane (Fig. 1 C). The distal part of the SDV membrane and the original plasma membrane were suggested to either remain as an extracellular layer protecting the silica (Fig. 1 D) or shed off to the environment (Fig. 1 E). Another model suggests localized membrane fusion at the apical part of the valve, followed by pulling of the distal SDV and original plasma membrane back into the cytoplasm at the valve edge (Fig. 1 F). In this last model, which is in accordance with classical exocytosis, the composition of the proximal SDV membrane is altered for its new function as the plasma membrane by incorporation of membranous vesicles (Fig 1 G). While none of these models have been unequivocally validated, fluorescently-tagged SDV membrane proteins in *Thalassiosira pseudonana* show rapid diffusion throughout the entire plasma membrane at the time of valve exocytosis, supporting the notion of (at least partial) integration of the SDV membrane into the plasma membrane[3,25].

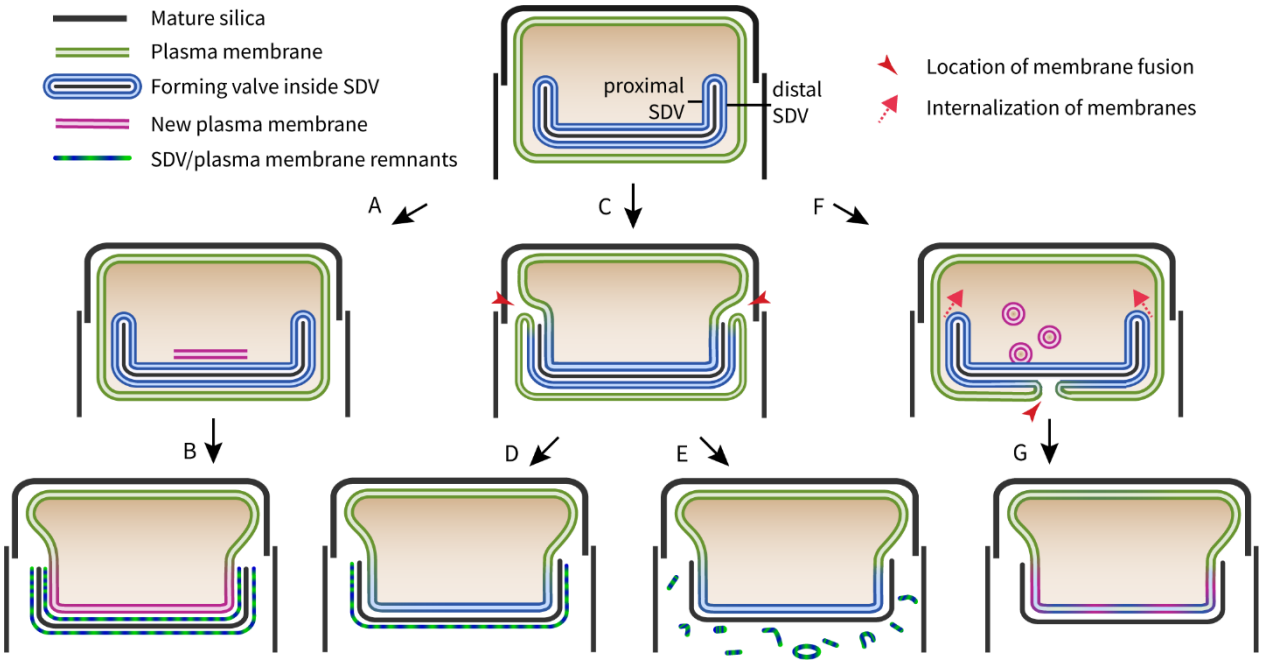

73 **Figure 1. Hypotheses for valve exocytosis in diatoms.** The middle row (**A**, **C**, **F**) shows three
74 different scenarios of valve release, and the bottom row (**B**, **D**, **E**, **G**) shows the subsequent fate of
75 the membranes in each of these scenarios. See text for details

76 Significant experimental challenges have hindered progress in solving the conceptual
77 problems of valve exocytosis, and in elucidating the dynamics and ultrastructure of the SDV. On
78 the one hand, traditional electron microscopy sample preparation for ultrastructural studies causes
79 artefacts like membrane shrinking and structure deformation[26]. On the other hand, the advantages
80 of light microscopy in studying the dynamic aspects of cell wall formation in living cells are limited
81 by the low spatial resolution and scarcity of molecular biology tools[27,28]. Due to these limitations,
82 *in situ* observations of the SDV in the cellular context are sparse, and direct evidence for the nature
83 of the silicification and exocytosis process is missing.
84 In this study, we investigated membrane dynamics during valve formation and exocytosis
85 in *Stephanopyxis turris* using a combination of transmission electron microscopy (TEM) and live-
86 cell confocal fluorescence microscopy. Compared to commonly studied diatom species, *S. turris* is
87 large and has easily discernible silica structures, allowing detailed observations of individual valves
88 and the dynamic development of their architectural features using fluorescence microscopy[29,30]. In
89 addition, state-of-the-art sample preparation methods for TEM result in excellent preservation of
90 subcellular structures, enabling investigation of the SDV in the near-native state at high resolution
91 without the distorting effects of traditional chemical fixation[31]. Using these methods, we show that
92 the SDV membrane tightly surrounds growing cell walls during the entire silicification process, and
93 that after valve exocytosis, external membranes slowly disintegrate, without signs of endocytic
94 retrieval or extracellular repurposing.
95

96 **Results**

97 *S. turris* cells are cylinders of about 50 µm long and 20 µm in diameter (Fig. 2 A). The cells contain
98 a large central vacuole, surrounded by a thin peripheral layer of cytoplasm filled with many small
99 chloroplasts. The cells form chains that are linked through tubular extensions of silica (labiate
100 processes) that extend from the apex of the valves (Fig. 2 B). When the cell walls are examined
101 using a scanning electron microscope (SEM), the two-layered structure of the valve is evident (Fig.

2 B, C). The proximal layer is thin and perforated by nano-sized pores, and is covered on the distal side by a more elevated layer that forms large polygons. The top of the polygonal layer is flattened, forming a 'T'-shape in cross-section.

Timing of cell wall formation is linked to the cell cycle. After cell division, each daughter cell inherits one half of the parental cell wall and forms a new valve (Supplementary Fig. 1). Directly after its exocytosis, the new valve is juxtaposed to the parental valve and covered by the parental girdle bands. The girdle bands are very thin and flexible such that some features of the underlying valve are visible, e.g a 'sheet' of girdle bands draped over the linking processes (Fig. 2 D, arrow). During the interphase, the cell grows in the longitudinal direction, pushing apart the two valves while girdle bands are added to cover the central part of the growing cell (Fig. 2 E, F).

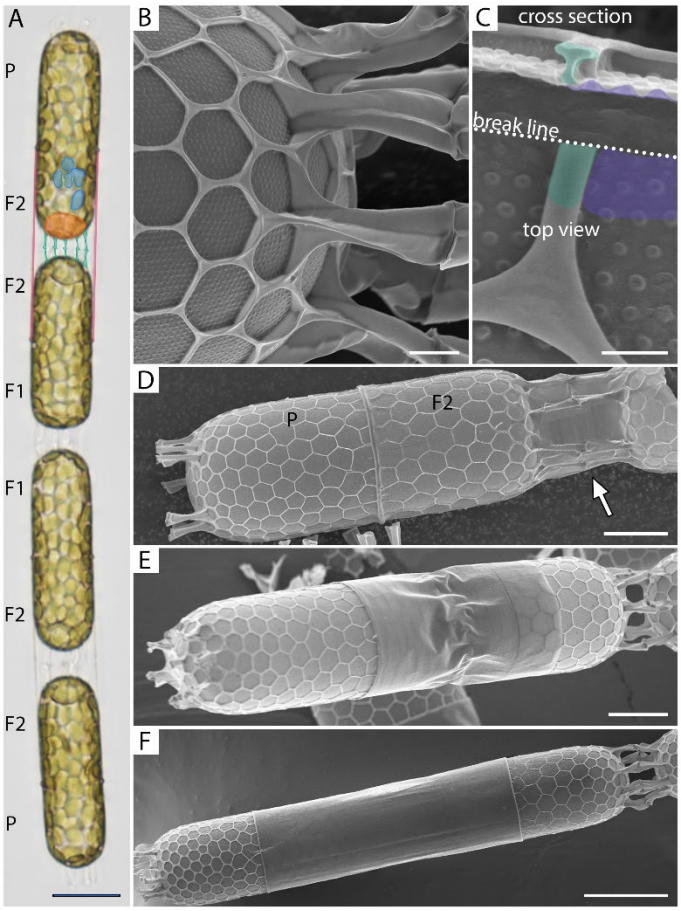

Figure 2. Cell architecture of *S. turris.* (**A**) Light microscope image of a chain of four cells connected through linking extensions (green). Each cell contains many yellow-brown chloroplasts

115 (blue). The two parental valves (P) are at the extremes of the chain, the two valves formed after the
116 first cell division (F1) are located in the center, and the four remaining valves (F2) are the youngest,
117 formed after the second cell division. Girdle bands (pink) cover the youngest valves. The nuclei
118 (orange) are located at the poles directly under the new valves (F2). Scale bar: 20 µm. (**B**) SEM
119 image of an apex of a valve, showing the polygonal pattern and linking extensions. Scale bar: 2
120 µm. (**C**) A fractured valve, revealing the T-shaped cross-section (green) of the polygonal silica layer
121 that is distal to the thinner perforated layer (purple). Scale bar: 500 nm. (**D-F**) Cells at different
122 stages of the cell cycle. (**D**) A cell with a new valve (F2, right) that is covered with parental girdle
123 bands (arrow) (P, left). Scale bar: 10 µm. (**E**) A cell during elongation and girdle band formation. As
124 valves were pushed apart, the midsection is covered only by girdle bands. Scale bar: 10 µm. (**F**)
125 Two daughter cells shortly after cell division, located under full-length girdle bands. Scale bar: 20
126 µm.

127 To study specific stages along the dynamic process of valve formation, we used previous
128 reports and established a protocol for *S. turris* cell cycle synchronization that is based on light
129 starvation[32,33]. For some diatoms, among which *S. turris*, extended dark period causes cell cycle
130 arrest in interphase, prior to the formation of new girdle bands[32]. When the culture is re-exposed
131 to light after 20 hours in the dark, the cells resume their cell cycle synchronously. Progression of
132 the diatom cell cycle can easily be monitored by visualizing the formation of new cell wall elements
133 using the fluorescent dye PDMPO[34]. PDMPO accumulates in the SDV and stains newly formed silica
134 (Fig. 3). After the end of light-starvation, the cells will first form their girdle bands and then the
135 valves (Fig. 3 A). The synchronized growth allowed us to calibrate time points at which the majority
136 of the cells are at specific stages of cell wall formation (Fig. 3 B, C). To study valve formation, the
137 cells were harvested 9 to 10 hours after the end of light starvation, when the synchronized culture
138 contains the highest proportion of cells at that stage.

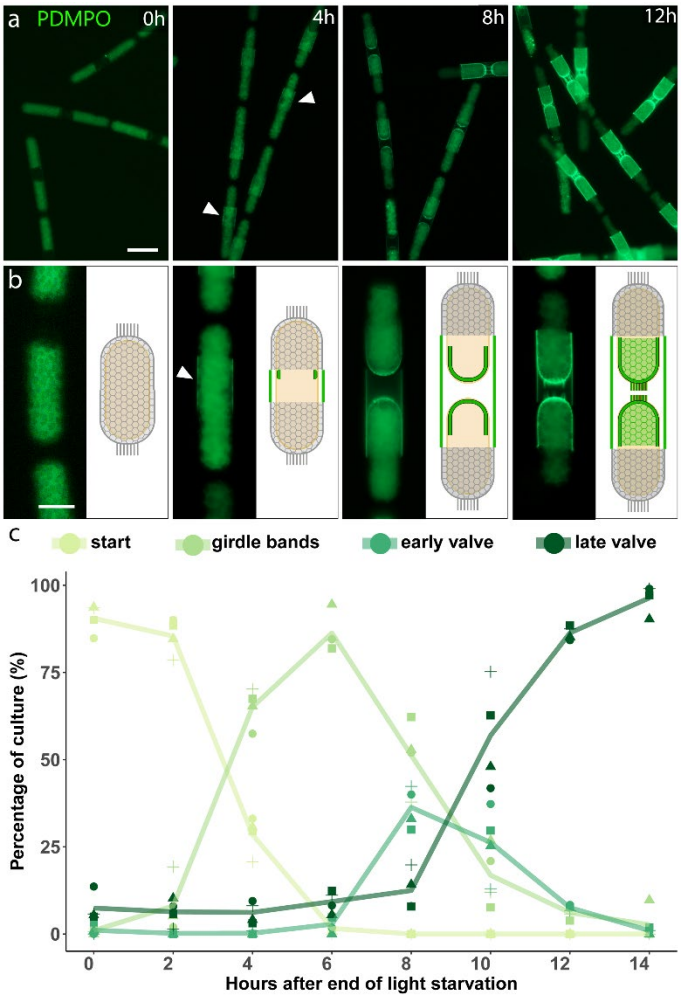

Figure 3. Light-induced synchronization of *S. turris* cell cycle. (**A**) Representative PDMPO fluorescence images of synchronized cultures, at various time points after the end of light starvation and addition of PDMPO. Shortly after the end of light starvation, none of the cells have fluorescently labelled silica, and only PDMPO fluorescence from within the vacuoles is visible. Four hours later, most cells have started forming girdle bands, visible as a fluorescent ring (arrowheads) around the cell. After eight hours, the majority of the culture is forming new, fluorescent valves. After twelve hours, nearly all cells have completed the formation of a new valve. Scale bar: 50 µm. (**B**) High magnification micrographs and schematics of single cells at key stages of cell wall formation. The key stages that are distinguished are: 'start', cells without PDMPO-labelled silica; 'girdle bands', cells during cell elongation and girdle band formation; 'early valve', after cell division, valve formation has started but is prior to growth of linking extensions; 'late valve', cells

at later stages of valve formation when polygons and extensions are visible. Scale bar: 20 µm (**C**) Percentage of cells at these four key stages during synchronized growth. The lines show the mean of four independent experiments, indicated with symbols. The highest percentage of cells that are forming valves is reached around nine hours.

To observe valve formation at a structural level, we used advanced sample preparation techniques for TEM. In short, synchronized cells were vitrified using high-pressure freezing and subsequently freeze-substituted and embedded in resin. These methods provide an optimal combination of near-native state preservation of subcellular structures paired with the ability of high-throughput room temperature imaging. The TEM images of *S. turris* cells prepared according to this procedure show exceptional preservation of the cellular environment, and in particular the SDV membranes and inorganic contents (Fig. 4).

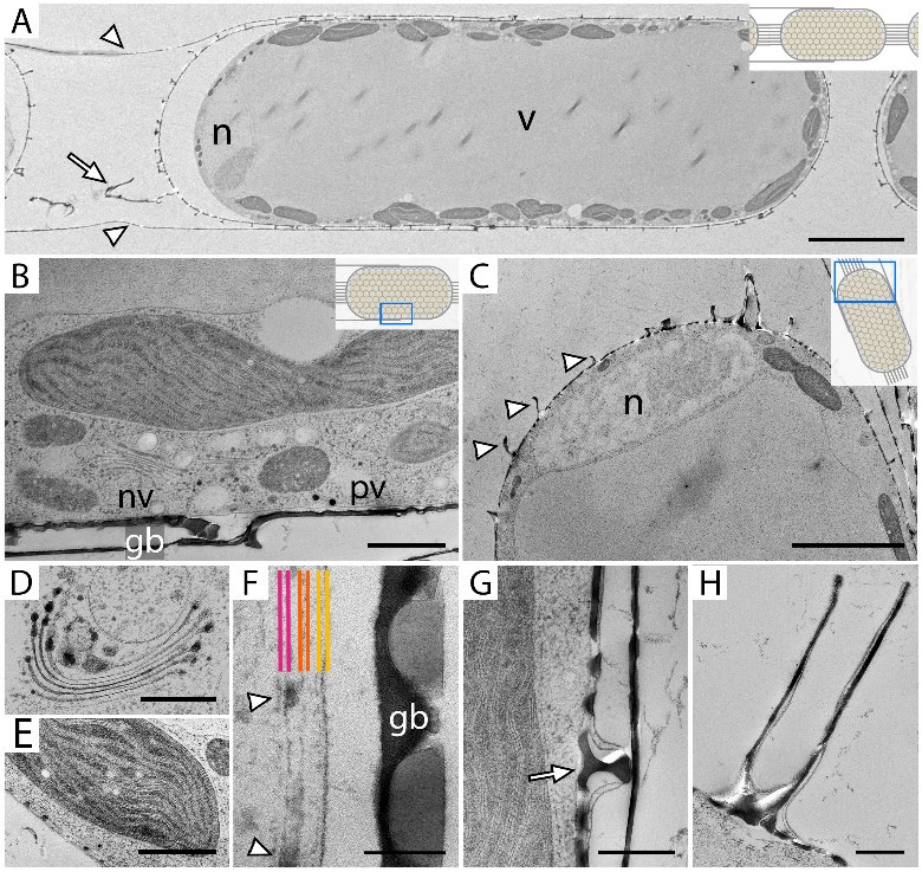

163 **Figure 4. Ultrastructural details of *S. turris* revealed by TEM imaging.** Insets indicate which
164 part of the cell is displayed. (**A**) A cross section through an entire cell, the nucleus (n), and the large
165 central vacuole (v) that is surrounded by darker chloroplasts are dominant. The silica cell wall (dark
166 contrast) is clearly visible at the left side, where the protoplast is not directly adjacent to the cell
167 wall due to slight plasmolysis. Arrowheads indicate girdle bands, and an arrow indicates a linking
168 extension. Scale bar: 10 µm. (**B**) The meeting point of a new valve (nv), and parental valve (pv) with
169 girdle bands (gb) attached to the latter. Scale bar: 1 µm. (**C**) Apex of a cell with the nucleus (n)
170 located directly under the valve. Silica protrusions indicated with arrowheads are cross sections of
171 the polygonal layer. Scale bar: 5 µm. **(D-H)** High magnification images of: (**D**) Golgi-body. Scale
172 bar: 500 nm. (**E**) Chloroplast. Scale bar: 1 µm. (**F**) SDV with growing silica (arrowheads). Bilayers of
173 the proximal SDV membrane (pink), distal SDV membrane (orange), and plasma membrane
174 (yellow) can be distinguished. Scale bar: 100 nm. (**G**) Fully formed polygon (arrow) still inside an
175 SDV. Scale bar: 500 nm. (**H**) Linking extension during its formation in an SDV. Scale bar: 500 nm.

176 By analysing hundreds of TEM images of synchronized cells at different stages of the cell
177 cycle, and categorizing and sorting these images, we established a timeline of valve formation and
178 exocytosis in *S. turris* (Fig. 5). Valve formation starts at the cell's apex, where the bilayer membranes
179 of the proximal and distal SDV membranes, as well as the plasma membrane, can be clearly
180 distinguished (Fig. 5 A-A''). With a distance of only 20 nm, the distal SDV membrane is in very close
181 proximity to the plasma membrane. Silica precipitation proceeds radially and the SDV expands
182 with it. After formation of the porous base layer, the polygonal layer is formed distally on top of
183 the base layer (Fig. 5 B-B''). The valve reaches its final morphology while it is still fully enclosed in
184 the SDV (Fig. 5 C-C''). During the entire silicification process, the SDV membrane tightly delineates
185 the growing valve, forming a highly confined space, in which the silica morphology is under the
186 control of the SDV membrane.
187 The details of the exocytosis process can be observed in the stages following valve
188 maturation. The first indication for exocytosis are isolated discontinuities in the distal membrane
189 coverage of the valve silica, even though the majority of the valve is still tightly surrounded by
190 membranes (Fig. 5 D-D''). From this moment, the membrane ultrastructure changes dramatically.
191 The tight delineation of the distal SDV and plasma membrane around the valve loosens, and we

observe deterioration of the structural integrity of the distal membranes (Fig 5 E-E''). The proximal SDV membrane is now continuous with the plasma membrane under the parental valve, forming the outermost surface that separates the cytoplasm from the cell's exterior, and thereby it is the new plasma membrane under the valve (Fig. 5 E'' arrow). At the end of this exocytosis process, the new valves can be recognized due to their position under the parental girdle bands. However, there are no visible traces of the old plasma and distal SDV membrane (Fig. 5 F-F'').

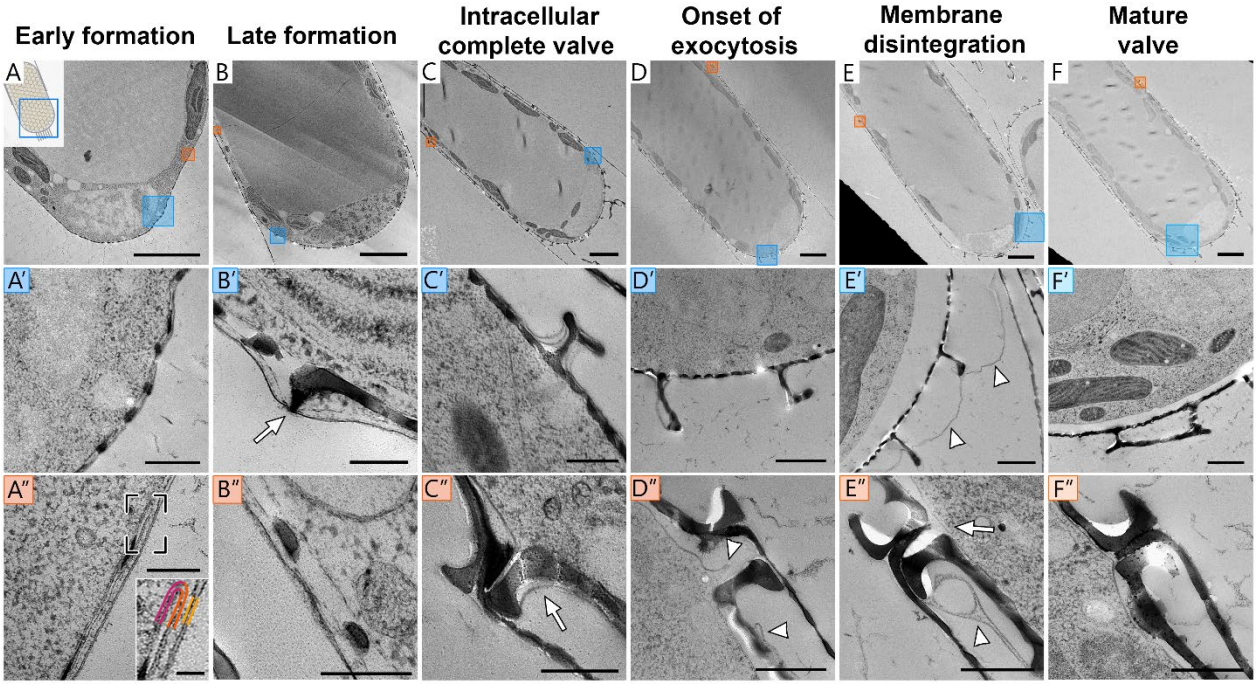

Figure 5. TEM images showing sequential stages of valve formation and exocytosis in *S. turris*. The top row shows a representative image of each stage, with higher magnification views of the boxed areas in the rows below. (**A**) Valve formation starts at the apex of the cell. (**A'**) Growing silica inside the SVD that is located directly under the plasma membrane. (**A''**) The SDV ends at the growing silica edge. The inset shows the bilayers of the proximal (pink) and distal (orange) SDV and the plasma membrane (yellow) in higher magnification. (**B**) Later during valve formation, (**B'**) the polygonal layer (arrow) is formed on top of the base layer, and (**B''**) the growing edge of the new valve has reached the edge of the parental valve. (**C**) Silicification of the new valve (arrow) is completed while it is still fully enclosed in the SDV. Mature valves can be recognized by (**C'**) the fully formed and flattened polygonal layer and (**C''**) pronounced hook shape at the valve edge. (**D**) At the onset of exocytosis, (**D'**) membranes still surround most parts of the new valve, (**D''**) but

210 they no longer form a complete enclosure (arrowheads). (**E**) Shortly after exocytosis, (**E'**) distal
211 membranes lose their structural integrity (arrowheads), and (**E''**) the plasma membrane is now
212 continuous (arrow) under the new valve. (**F-F''**) After completion of exocytosis, there are no traces
213 left of the distal membrane remnants. Scale bars represent 5 µm (**A, B, C, D, E, F**), 1 µm (**D', E', F'**),
214 500 nm (**A', C', C'', D'', E'', F''**), 200 nm (**A'', B', B'', C' inset**) and 50 nm (**A'' inset**).

215 The high-resolution structural observations using electron microscopy strongly suggest
216 that valve exocytosis involves degradation of the distal membranes in the extracellular
217 environment (Fig. 1 E). However, these are 2D frozen snapshots that do not reveal direct and
218 dynamic information about the exocytosis process. Therefore, we investigated the process
219 dynamics in living cells using time-lapse confocal microscopy. Synchronized cultures were labelled
220 with PDMPO to visualize newly formed silica, and with FM4-64 to stain the plasma membrane.
221 FM4-64 is an amphiphilic, membrane-impermeable dye, that can enter the cell only via endocytic
222 vesicles[35,36]. We followed doubly-labelled cells during valve formation at 20 to 40 minute intervals.
223 As the cells are sensitive to these imaging conditions we were able to record cells at only 2-5 time
224 points. Some cells showed the initial stages of silica deposition (Fig. 6 A-C), whereas other were
225 captured during valve exocytosis (Fig. 6 D-E).

226 In accordance with the TEM images, live-cell imaging showed that silica deposition starts
227 at the cell apex and radiates towards the valve edge (Fig. 6 A-B). The outlines of the growing
228 polygonal layer can be distinguished in the FM4-64 channel since the plasma membrane is tightly
229 outlining the growing silica structures within the SDV (Fig. 6 B), and the silicification of the linking
230 extensions is preceded by membrane extension (Fig. 6 C'', arrowheads). In cells that were imaged
231 from completion of the valve onwards, recently formed linking extensions still have membranes
232 tightly surrounding them at the initial time point of imaging (Fig. 6 D). However, the membranes
233 have largely disintegrated a few hours later, only leaving some FM4-64 stained remnants where
234 the linking extensions connect to each other (Fig. 6 E).

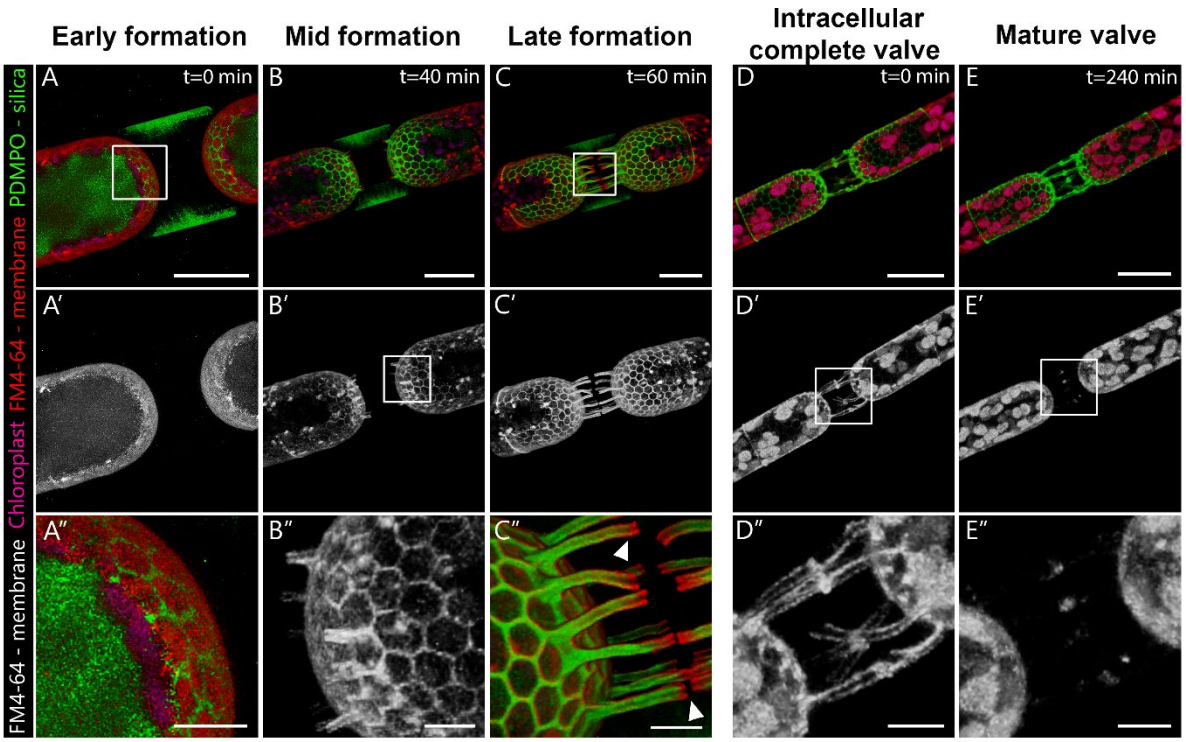

Figure 6. Coordinated silica and membrane dynamics during valve formation in *S. turris* revealed by 3D reconstructions of time-lapse confocal fluorescence images. (**A-E**) Images show an overlay of the fluorescence signals from two cells at different stages of valve formation. (**A-C**) A cell during valve formation. During early valve formation, the emerging silica polygons at the apex can be seen by PDMPO staining (**A**). Later on, membranes can be seen outlining the growing polygons and linking extensions (**B**). The growth of linking extensions is led by a membrane outlining their shape (**C**, arrowheads). (**D-E**) A different cell shortly before (**D**) and after exocytosis (**E**) of a mature valve. **A′-E′** show only the FM4-64 fluorescence highlighted in white. (**A′′-E′′**) Higher magnification of the boxed area in A, B′, C, D′, and E′. Scale bars represent 20 µm (**A-E′**) and 5 µm (**A′′-E′′**).

In order to follow the entire valve formation process in the same cell, some adjustments were made to the imaging protocol. Most importantly, PDMPO imaging was omitted to minimize laser damage, and the concentration of FM4-64 was reduced. This improved protocol enabled us to record the membrane dynamics during the entire process of valve formation and exocytosis at a higher temporal resolution (Fig. 7, Supplementary video 1). At the beginning, formation of the valves is perceptible because the plasma membrane outlines the growing polygons and linking

252 extensions (Fig. 7 A, t=0 to t=126). Exocytosis of the completed valves is manifested by clear
253 changes to the membrane arrangement (the valve at the top is exocytosed first, between t=126
254 and t=138, and the second valve is exocytosed around t=168). First, loosening of the plasma
255 membrane – SDV – silica complex is evident as the labelled plasma membrane no longer outlines
256 the polygons. At the same time point, we observe a slight enhancement of the fluorescent signal,
257 possibly because a fusion between the plasma and SDV membranes allows free FM4-64 from the
258 medium to infiltrate and stain the SDV. Recently exocytosed valves remain temporarily surrounded
259 by the distal membranes, which gradually disintegrate. These membrane remnants, which are
260 visible both in the TEM and live-cell images, gradually lose their tight delineation of the valve
261 structures. This is most evident around the linking extensions as these are located relatively far
262 away from the cell body. In some cases, it is clear that the membranes surrounding a linking
263 extension are no longer connected to the cell body (Fig. 7 B, Supplementary Fig. 2). This labelling
264 pattern confirms that major fractions of the external membranes are completely detached from
265 the main cell surface, and that exocytosis of the valve is accompanied by massive membrane
266 shedding into the extracellular space. Additionally, we can rule out the possibility of significant
267 retrieval of the external membranes into the cell as such a scenario would result in excess FM4-64
268 labeling within the cell.

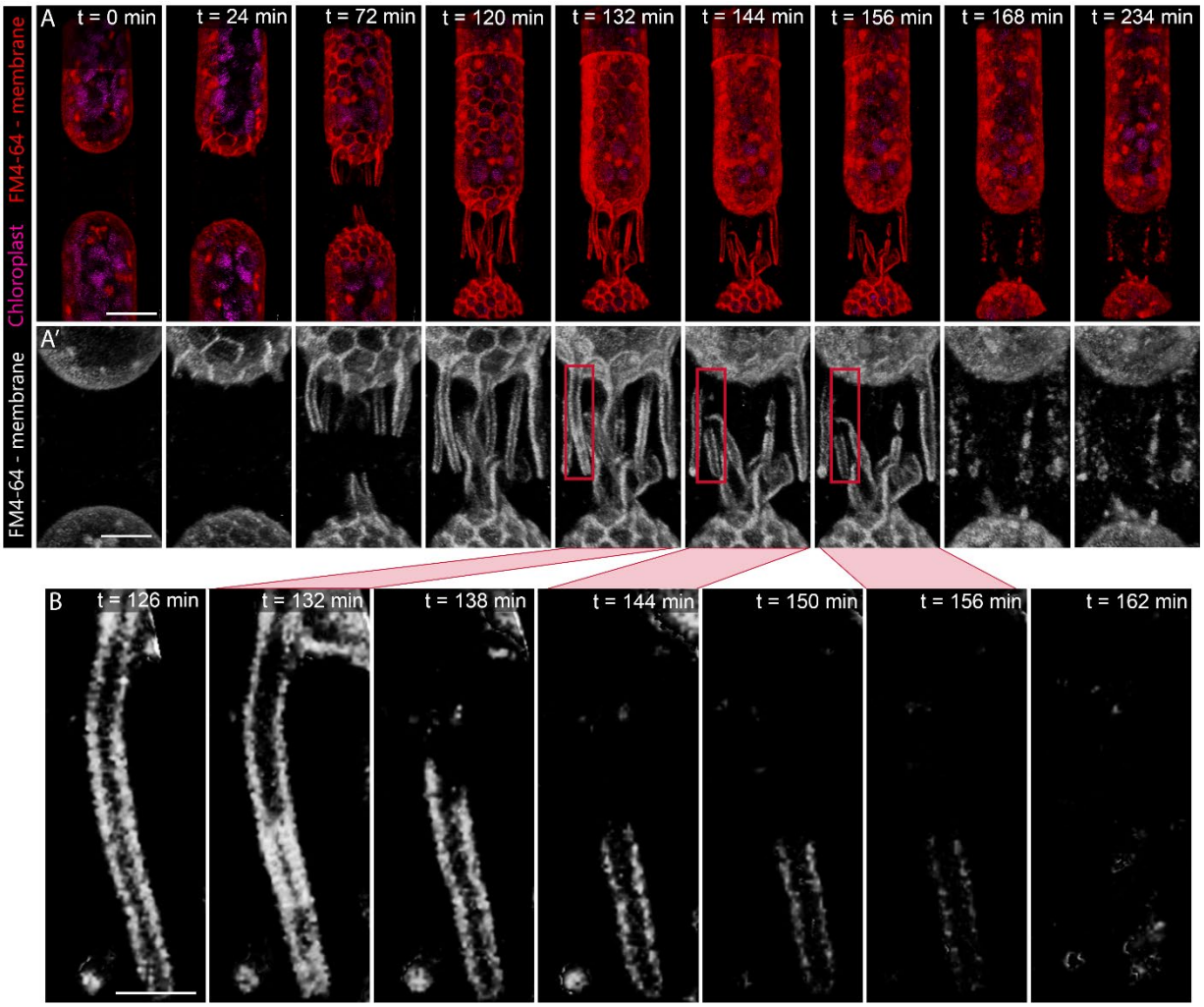

Figure 7. Membrane dynamics in a living *S. turris* cell going through valve formation and exocytosis. (**A**) 3D reconstructions of time-lapse confocal fluorescence images of FM4-64 (plasma membrane - red) and chloroplast autofluorescence (magenta). (**A'**) The same images as in (**A**) with only membrane staining (FM4-64) highlighted in white at higher magnification. (**B**) Cropped area around one linking extension (indicated with boxes in **A'**). Onset of exocytosis of the valve on top is between t=126 and 132, after which the membrane remnants around the linking process are no longer connected to the cell and disintegrate gradually. Scale bars: 10 µm (**A**), 5 µm (**B**) and 2 µm (**C**).

280 **Discussion**

281 Extrusion of the intracellularly formed, rigid cell walls of diatoms is an extraordinary exocytosis
282 event, which is difficult to reconcile with known exocytosis processes. The combination of
283 ultrastructural studies and live-cell imaging allowed us to investigate the membrane dynamics
284 during valve formation and exocytosis in *S. turris*. Our observations of the SDV ultrastructure show
285 that the intricate silica patterns are formed within a tightly confined space, bound by the SDV
286 membrane, supporting the idea that the SDV membrane is controlling the shape of growing silica
287 structures[37,38]. Furthermore, we provide a direct evidence from living cells for the actual exocytosis
288 mechanism. Our data show that the valve is exocytosed through fusion of the plasma membrane
289 and proximal SDV membrane, and that the distal membranes surrounding recently exocytosed
290 valves gradually disintegrate after exocytosis (Figs. 5, 7). Altogether, our results indicate that
291 exocytosis of diatom silica involves two remarkable events. First, the repurposing of an organelle
292 membrane into a plasma membrane (Fig. 1 C) and second, the shedding of a huge amount of
293 membranes (Fig. 1 E).

294 The first event, conversion of the proximal SDV membrane into a new plasma membrane,
295 requires regulated fusion of the SDV and the old plasma membrane. As the SDV and plasma
296 membranes carry out specialized, different tasks, it is likely that both require unique lipid and
297 protein compositions, which need to be adjusted after fusion[39]. The TEM data suggest multiple
298 fusion events all around the valve edge, resulting in the proximal SDV membrane becoming the
299 new outermost boundary of the cytoplasm. Subsequently, additional fusion events distally to the
300 valve might serve to break-up the distal SDV membrane and the old plasma membrane. Fusion of
301 the SDV and plasma membrane at the time of valve exocytosis was demonstrated previously in
302 live-cell studies of *T. pseudonana*[3,25], implying a general exocytosis strategy.

303 Regarding the second point, our results show that the distal membranes disintegrate
304 gradually while they are no longer connected to the cell membrane (Fig. 7, Supplementary Fig. 2).
305 Therefore, internalization of these membranes through compensatory endocytosis or
306 macropinocytotic-like invagination is ruled out. FM4-64 attaches only transiently to membrane
307 lipids, and can rapidly diffuse out from the degrading debris into the surrounding medium, where
308 its fluorescence is significantly reduced[35]. Therefore, we cannot identify the fate of these

309 membrane remnants. Important to note is that the parental girdle bands form a quasi-enclosed
310 compartment around the newly formed valves, possibly slowing down diffusion away from the cell
311 and facilitating the uptake of the membrane debris for cellular use after disintegration. On first
312 sight, this exocytosis process including the extracellular disintegration of large amounts of
313 membrane appears costly to the cell, but it is conceivable that the costs are minimized by recycling
314 the building blocks from within the space enclosed by the girdle bands.

315 Exocytosis is an essential cellular process that has been widely studied in a variety of model
316 systems. In the classical secretory exocytosis systems, the process proceeds via large amounts of
317 small vesicles that fuse with the membrane[40]. Nevertheless, there are known alternatives related
318 to larger exocytosis needs. For example, giant vesicles in the *Drosophila* salivary glands squeeze
319 out their viscous cargo through a wide pore by crumpling of the vesicular membrane, followed by
320 membrane retrieval by small endocytic vesicles[41]. In the acrosome reaction, the plasma membrane
321 and distal acrosomal membrane fuse at several locations forming vesicles that are dispersed in the
322 environment while the proximal acrosomal membrane remains intact and becomes the new
323 boundary that separates the spermatozoa from the environment[42,43]. Exocytosis of diatom cell
324 walls is a parallel strategy to these examples, adapted to account for the need to extrude a rigid,
325 large vesicle content.

326 To conclude, this work proposes a remarkable mechanism for the exocytosis of the giant
327 silica deposition vesicle during silicification in diatoms. The size of the studied unicellular alga,
328 together with advanced fluorescent and electron microscopy, facilitated the elucidation of the
329 exocytosis steps. With the toolbox for genetic research in diatom growing, it will soon be possible
330 to investigate whether similar conserved processes are involved in the regulation of this event as
331 in classical exocytosis.

332

333

334

335

336

337

338 **Materials and methods**

339 *Cell cultures*

340 *S. turris* was isolated from the North Sea in 2004 and provided by the group of Prof. Eike Brunner,
341 TU Dresden. *S. turris* cultures were maintained in natural Mediterranean seawater that was filtered,
342 its salinity corrected to 3.5% and supplemented with f/2 nutrient recipe. Cultures were maintained
343 at 18°C under 16/8 hours light/dark cycles, by a weekly dilution of 5 ml from a parent culture into
344 45 ml fresh medium.

345 *Cell cycle synchronization*

346 For synchronization of the cell cycle, 5 ml of a mature cell culture was used to start a new 50 ml
347 culture. After 48 hours of growth under the normal 16L/8D cycle, the culture was placed in
348 darkness for 20 hours. After 20 hours of darkness, the culture was again exposed to light. To track
349 the formation of new silica, PDMPO [2-(4-pyridyl)-5-((4-(2-dimethylaminoethyl-amino-
350 carbamoyl)methoxy)-phenyl)oxazole] (ThermoFisher Scientific, USA) was added to a final
351 concentration of 330 µM. PDMPO fluorescence was monitored by imaging the cultures with an
352 epifluorescence microscope (Nikon Eclipse Ni-U, ex: 365 em: 525). Four cultures were imaged (at
353 least 100 cells per time point) every 2 hours until all of the cells had formed new valves (about 14
354 hours).

355 *Sample preparation for SEM*

356 Cells were prepared for SEM in two different ways. For the first, quick method, 10 µl of culture was
357 pipetted onto polycarbonate Whatman® Nuclepore™ Track-Etched membranes, which were then
358 dried using a vacuum filter. To prepare cells in which the girdle band region does not collapse, the
359 second method uses critical point drying (CPD). To prepare cells for CPD, cells were fixed in a
360 solution of 2% Glutaraldehyde and 4% Paraformaldehyde in artificial seawater for 1 hour at room
361 temperature while shaking. Then cells were washed 3 times with deionized water (Milli-Q® IQ
362 7003 Ultrapure Lab Water System, Merck), and dehydrated by washing them in a graded series of
363 ethanol. The final wash was done in 100% anhydrous ethanol overnight. The dehydrated samples

364 were then dried in a critical point dryer using liquid CO_2 as transitional fluid. The Track-Etched
365 membranes or dried cells were then placed onto a conductive carbon tape on an aluminium stub.

366 *SEM imaging*

367 The samples were sputter-coated with 4 nm iridium (Safematic). The dried and coated cell wall
368 samples were imaged with Sigma 500 or Ultra 55 FEG scanning electron microscopes (Zeiss,
369 Germany), using 3-5 kV, aperture size 20-30 um and a working distance of about 3 mm.

370 *Sample preparation for TEM*

371 To preserve the cells in the native state they were cryo-fixed, using high pressure freezing (HPF),
372 followed by freeze substitution (FS), according to previously published protocols [31,44]. HPF ensures
373 rapid vitrification of the cells preventing the formation of ice crystals, which would damage cellular
374 structures. Through FS, the vitrified ice is replaced with an organic solvent and fixatives.
375 Synchronized cultures were harvested by collecting the cells on a 5 µm filter membrane. The cells
376 were collected from the membrane by washing them into an Eppendorf tube using 200 µl of
377 seawater. After letting the cells sediment for 10 minutes, 2 µl aliquots were pipetted into aluminium
378 discs (Wohlwend GmbH, Sennwald, Switzerland) and directly loaded into a Leica ICE high pressure
379 freezing machine (Leica Microsystems GmbH, Wetzlar, Germany). The samples were vitrified in
380 liquid nitrogen (−192 °C) at 210 MPa (2048 bar). The vitrified samples were stored in liquid nitrogen
381 until freeze-substitution in an EM ASF2 (Leica Microsystems GmbH, Wetzlar, Germany). The
382 vitrified water in the sample was substituted with an organic solvent, 100% anhydrous acetone, at
383 (−90 °C). The acetone was supplemented with chemical fixatives (0.2% uranyl acetate and 0.2%
384 osmium tetroxide) to enhance cross-linking and contrast of cellular structures. The samples were
385 immersed in the solution for 48 hours at −90 °C. Then, the samples were allowed to gradually
386 warm for 24 hours to -20°C, and then gradually warmed to 0°C during one hour. The samples were
387 washed 3 times with acetone. Then the acetone was replaced with Epon (Agar Scientific Ltd,
388 Stansted, U.K.) using gradient concentration mixtures (10%, 20%, 30%, 40%, 60%, 80%, 100% Epon
389 in acetone), twice a day at room temperature. The sample in 100% Epon was hardened at 70 °C
390 for 72 h. Ultrathin sections of 70 nm were sliced using an ultra-microtome (Ultracut UCT, Leica
391 Microsystems GmbH, Wetzlar, Germany) equipped with a diamond knife (Ultra 45°, Diatome Ltd,

392 Nidau, Switzerland). The sections were picked up onto copper TEM grids, coated with carbon film.
393 The sections were then post-stained by placing them onto a drop of lead citrate solution. After
394 three minutes of staining, the grids were washed three times in drops of water and then dried by
395 blotting onto whatman filter paper. In total, we prepared 16 frozen samples that were further
396 processed using freeze substitution during 3 different cycles, and subsequently imaged hundreds
397 of cells.

398 *TEM imaging*

399 The TEM samples were imaged with a Tecnai Spirit transmission electron microscope (FEI,
400 Eindhoven, Netherlands) operated at 120 kV and equipped with Gatan Oneview 4 k × 4 k camera
401 (Gatan Inc., Pleasanton, U.S.A.).

402 *Live cell imaging*

403 For single-cell time-lapse imaging, a culture was synchronized and stained with PDMPO (330 μM).
404 About 8 hours after the end of light starvation, when most cells had gone through cytokinesis, an
405 aliquot of 100 μl was taken and FM4-64 (ThermoFisher Scientific, USA) was added to a final
406 concentration of 4-8 μM to stain the membranes. After adding the membrane dye, a 20 μl drop
407 was mounted on a microscope slide and covered with a glass coverslip, using dental wax as spacer.
408 The samples were visualized using a Leica TCS SP8-STED confocal microscope equipped with a
409 HCS PL APO 86x/1.20W motCORR objective. FM4-64 and chlorophyll autofluorescence were
410 acquired by white-light laser using 550 nm laser line (6% laser power) and 650 nm laser line (7%
411 laser power), respectively. PDMPO fluorescence was acquired using a 405 nm laser (5% laser
412 power). HyD-SMD detectors were used for PDMPO and FM4-64 with emission collection width set
413 to 474-530 and 608-640 nm, respectively. Chlorophyll autofluorescence emission was collected
414 using a HyD detector with 741-779 nm detection width and the transmission channel was detected
415 with a PMT detector. The cells were imaged for 2 to 4 hours at intervals of 3 to 60 minutes. Images
416 were analysed using Leica Application Suite X. In total, Time lapses from over 50 cells were
417 collected over the entire period.

418

419 **Acknowledgements**

420 We thank Anne Jantschke and Nathalie Pytlik from TU Dresden for providing cultures. We thank
421 Simon Michaeli from the Volcani Institute (ARO) for his contribution in finding the right live cell
422 imaging platform. This project has received funding from the European Research Council (ERC)
423 under the European Union's Horizon 2020 research and innovation programme (grant agreement
424 No. 848339). D. dH. was supported by the Sustainability and Energy Research Initiative (SAERI) of
425 Weizmann Institute of Science.

426 **Data availability**

427 All data generated or analysed during this study are included in the manuscript and supporting
428 file; Source Data files for Figures 2-7 have been deposited to Dryad.

429 **Additional information**

430 Supplementary Information accompanies this paper at https://doi.org/XXX.XXX

431 **Competing interests**

432 The authors declare no competing interests.

433 **References**

434 1. Armbrust, E. V. The life of diatoms in the world's oceans. *Nature* **459**, 185–192 (2009).
435 2. Kroger, N. & Poulsen, N. Diatoms — From Cell Wall Biogenesis to Nanotechnology. *Annu.*
436 *Rev. Genet.* **42**, 83–107 (2008).
437 3. Kotzsch, A. *et al.* Silicanin-1 is a conserved diatom membrane protein involved in silica
438 biomineralization. *BMC Biol.* **15**, (2017).
439 4. Kröger, N., Deutzmann, R. & Sumper, M. Polycationic peptides from diatom biosilica that
440 direct silica nanosphere formation. *Science (80-.).* **286**, 1129–1132 (1999).
441 5. Sumper, M., Brunner, E. & Lehmann, G. Biomineralization in diatoms: Characterization of
442 novel polyamines associated with silica. *FEBS Lett.* **579**, 3765–3769 (2005).
443 6. Hildebrand, M. Diatoms, Biomineralization Processes , and Genomics. *Chem. Rev.* **108**,
444 4855–4874 (2008).

445 7. Drum, R. W. & Pankratz, H. S. Post mitotic fine structure of Gomphonema parvulum. *J.*
446 *Ultrasructure Res.* **10**, 217–223 (1964).
447 8. Heintze, C. *et al.* An intimate view into the silica deposition vesicles of diatoms. *BMC*
448 *Mater.* **2**, 1–15 (2020).
449 9. Mayzel, B., Wolf, S. G., Varsano, N. & Gal, A. Extracellular silica formation by diatoms.
450 10. Hildebrand, M., Lerch, S. J. L. & Shrestha, R. P. Understanding Diatom Cell Wall
451 Silicification — Moving Forward. *Front. Mar. Sci.* **5**, 1–19 (2018).
452 11. Kröger, N., Lorenz, S., Brunner, E. & Sumper, M. Self-assembly of highly phosphorylated
453 silaffins and their function in biosilica morphogenesis. *Science (80-.).* **298**, 584–586 (2002).
454 12. Scheffel, A., Poulsen, N., Shian, S. & Kröger, N. Nanopatterned protein microrings from a
455 diatom that direct silica morphogenesis. *Proc. Natl. Acad. Sci.* **108**, 3175–3180 (2011).
456 13. Montagna, M. *et al.* Interactions of long-chain polyamines with silica studied by molecular
457 dynamics simulations and solid-state NMR spectroscopy. *Langmuir* **36**, 11600–11609
458 (2020).
459 14. Jantschke, A. *et al.* Insight into the Supramolecular Architecture of Intact Diatom Biosilica
460 from DNP-Supported Solid-State NMR Spectroscopy. *Angew. Chemie Int. Ed.* **54**, 15069–
461 15073 (2015).
462 15. Stoermer, E. F., Pankratz, H. S. & Bowen, C. C. Fine Structure of the Diatom Amphipleura
463 pellucida. II. Cytoplasmic Fine Structure and Frustule Formation. **52**, 1067–1078 (1965).
464 16. Battey, N. H., James, N. C., Greenland, A. J. & Brownlee, C. Exocytosis and Endocytosis.
465 *Plant Cell* **11**, 643–659 (1999).
466 17. Schulz, D. Das Schicksal von Silicalemma und Plasmalemma während der Zellwandbildung
467 bei Coscinodiscus granii Gough und Thalassiosira eccentrica (Ehrenb.) Cleve. *Ber. Dtsch.*
468 *Bot. Ges.* **97**, 411–419 (1984).
469 18. Volcani, B. E. Cell Wall Formation in Diatoms: Morphogenesis and Biochemistry. in *Silicon*
470 *and Siliceous Structures in Biological Systems* 157–200 (Springer, 1981).
471 19. Bedoshvili, Y. D. *et al.* Frustule morphogenesis of raphid pennate diatom Encyonema
472 ventricosum (Agardh) Grunow. *Protoplasma* **255**, 911–921 (2018).
473 20. Chiappino, M. L. & Volcani, B. E. Studies on the Biochemistry and Fine Structure of Silicia

Shell Formation in Diatoms VII. Sequential Cell Wall Development in the Pennate Navicula pelliculosa. *Protoplasma* **93**, 205–221 (1977).

21. Crawford, R. M. Valve Formation in Diatoms and the Fate of the Silicalemma and Plasmalemma. *Protoplasma* **106**, 157–166 (1981).

22. Dawson, P. A. Observations on the structure of some forms of Gomphonema Parvulum Kutz. III. Frustule formation. *J. Phycol.* **9**, 353–365 (1973).

23. Reimann, B. E. F., Lewin, J. C. & Volcani, B. E. Studies on the Biochemistry and fine structure of silica shell formation in diatoms I. The Structure of the Cell Wall of Cylindrotheca fusiformis. *J. Cell Biol.* **24**, 39–55 (1965).

24. Schmid, A.-M. M. Wall Morphogenesis in Coscinodiscus wailesii. *8th Diatom Symp.* 293–314 (1984).

25. Yee, D. P., Hildebrand, M. & Tresguerres, M. Dynamic subcellular translocation of V-type H+-ATPase is essential for biomineralization of the diatom silica cell wall. *New Phytol.* **225**, 2411–2422 (2020).

26. Li, C. W. & Volcani, B. E. Studies on the Biochemistry and Fine Structure of Silica Shell Formation in Diatoms. X Morphogenesis of the Labiate Process in Centric Diatoms. *Protoplasma* **124**, 147–156 (1985).

27. Gröger, P., Poulsen, N., Klemm, J., Kröger, N. & Schlierf, M. Establishing super-resolution imaging for proteins in diatom biosilica. *Sci. Rep.* **6**, 1–8 (2016).

28. Kroth, P. G. *et al.* Genome editing in diatoms: achievements and goals. *Plant Cell Rep.* **37**, 1401–1408 (2018).

29. Chepurnov, V. A. *et al.* In search of new tractable diatoms for experimental biology. *BioEssays* **30**, 692–702 (2008).

30. von Stosch, H. A. & Drebes, G. Entwicklungsgeschichtliche Untersuchungen an zentrischen Diatomeen IV. *Helgoländer Wissenschaftliche Meeresuntersuchungen* **11**, 209–257 (1964).

31. Kadan, Y. *et al.* In situ electron microscopy characterization of intracellular ion pools in mineral forming microalgae. *J. Struct. Biol.* **210**, 107465 (2020).

32. Brzezinski, M. A., Olson, R. J. & Chisholm, S. W. Silicon availability and cell-cycle progression in marine diatoms. *Mar. Ecol. Prog. Ser.* **67**, 83–96 (1990).

503 33. Vaulot, D., Olson, R. J. & Chisholm, S. W. Light and dark control of the cell cycle in two
504 marine phytoplankton species. *Exp. Cell Res.* **167**, 38–52 (1986).
505 34. Shimizu, K., Del Amo, Y., Brzezinski, M. A., Stucky, G. D. & Morse, D. E. A novel fluorescent
506 silica tracer for biological silicification studies. *Chem. Biol.* **8**, 1051–1060 (2001).
507 35. Bolte, S. *et al.* FM-dyes as experimental probes for dissecting vesicle trafficking in living
508 plant cells. *J. Microsc.* **214**, 159–173 (2004).
509 36. Kühn, S. F. & Brownlee, C. Membrane organisation and dynamics in the marine diatom
510 Coscinodiscus wailesii (Bacillariophyceae). *Bot. Mar.* **48**, 297–305 (2005).
511 37. Tesson, B. & Hildebrand, M. Extensive and intimate association of the cytoskeleton with
512 forming silica in diatoms: Control over patterning on the meso- and micro-scale. *PLoS*
513 *One* **5**, (2010).
514 38. Van de Meene, A. M. L. & Pickett-Heaps, J. D. Valve morphogenesis in the centric diatom
515 Proboscia alata Sundstrom. *J. Phycol.* **38**, 351–363 (2002).
516 39. Holthuis, J. C. M. & Menon, A. K. Lipid landscapes and pipelines in membrane
517 homeostasis. *Nature* **510**, 48–57 (2014).
518 40. Gundelfinger, E. D., Kessels, M. M. & Qualmann, B. Temporal and spatial coordination of
519 exocytosis and endocytosis. *Nat. Rev. Mol. Cell Biol.* **4**, 127–139 (2003).
520 41. Kamalesh, K. *et al.* Exocytosis by vesicle crumpling maintains apical membrane
521 homeostasis during exocrine secretion. *Dev. Cell* **56**, 1603-1616.e6 (2021).
522 42. Okabe, M. The Acrosome Reaction: A Historical Perspective. in *Sperm Acrosome*
523 *Biogenesis and Function During Fertilization* (ed. Buffone, M. G.) 1–13 (Springer
524 International Publishing, 2016). doi:10.1007/978-3-319-30567-7_1
525 43. Tomes, C. N. Acrosomal Exocytosis. in *Molecular Mechanisms of Exocytosis* 117–147
526 (Springer New York, 2007). doi:10.1007/978-0-387-39961-4_9
527 44. Weston, A. E., Armer, H. E. J. & Collinson, L. M. Towards native-state imaging in biological
528 context in the electron microscope. *J. Chem. Biol.* **3**, 101–112 (2010).
529
530
531

Supplementary information

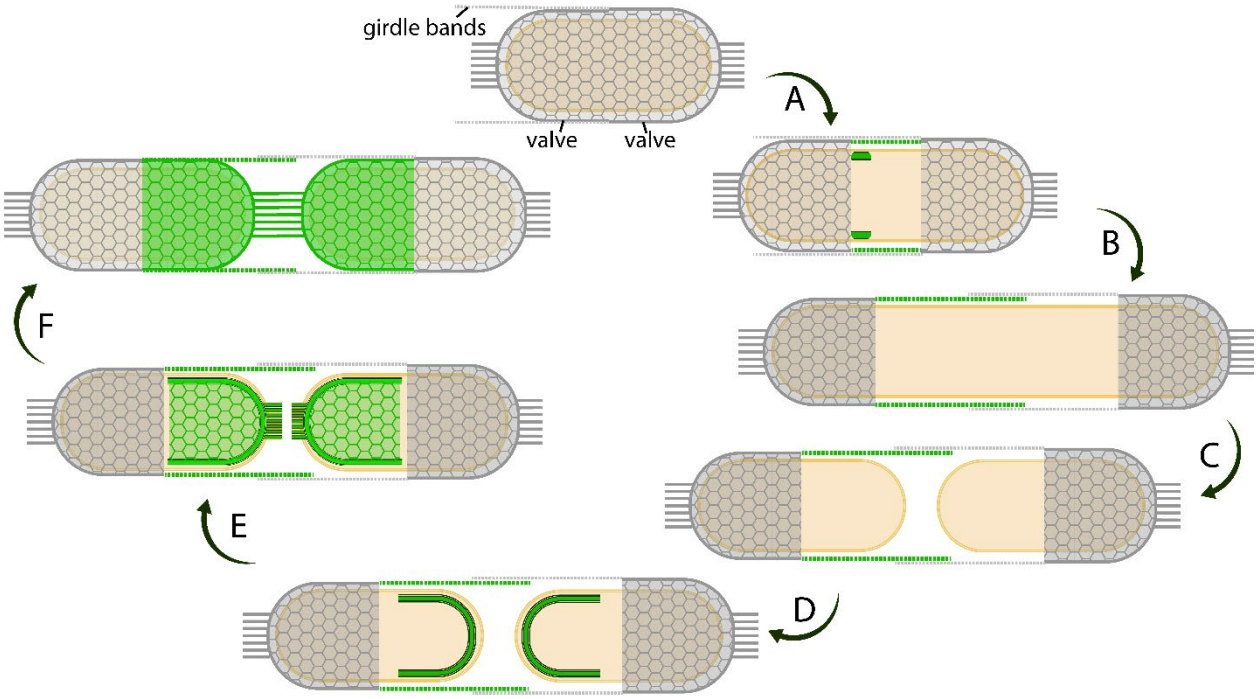

Supplementary figure 1. Cell cycle of *S. turris*. New silica elements, formed during the current cell cycle are coloured green. Dashed lines represent girdle bands. (**A**) Start of a cell cycle with a protoplast enclosed by the two parental valves, the valve edges are directly adjacent to each other. The older valve is on the right, and the younger valve on the left. The younger valve is covered under the girdle bands of the older valve. (**B**) Protoplast starts growing in preparation for the next cell division. As the silica valves are rigid and not elastic, growth is only possible in longitudinal direction by pushing apart the two valves. New girdle bands (green) are formed in individual SDVs and added to the edge of the younger valve. (**C**) After the protoplast has reached its final length, the cell undergoes cytokinesis, resulting in two daughter cells enclosed in the parental cell wall.

549 (**D**) Each daughter cell inherits one half of the parental cell wall and starts forming a new valve,
550 inside an SDV, shortly after cell division. (**E**) The new valves are completed with attachment of the
551 linking extensions, after which they are exocytosed. (**F**) Both daughter cells are now ready to
552 continue to the next cell cycle.

553 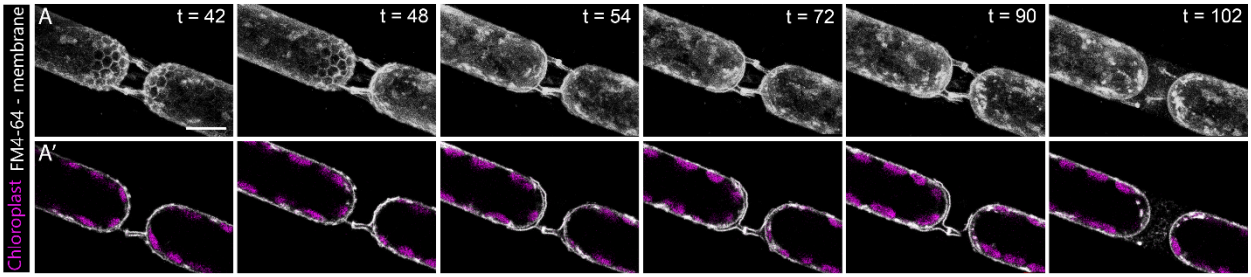

554 **Supplementary figure 2. Distal membranes that undergo degradation are disconnected**
555 **from the cellular membrane.** Representative (**A**) maximum intensity projections and (**A'**) single
556 z-slices of time-lapse confocal fluorescence images. Images show membrane staining (FM4-64) in
557 white and chloroplasts autofluorescence in magenta. The elapsed time since the start of imaging
558 (in minutes) is shown on the upper right corner. Exocytosis of the valve on the bottom right starts
559 between t=42 and t=48. The valve on the top left is exocytosed between t=48 and t=54. In t=72
560 and t=90, distal membranes around the valve are not connected to the cellular membrane. At
561 t=102 the remnants have largely disintegrated. Scale bar: 10 µm
562
563
564
565 **Supplementary video 1.** Time-lapse imaging video of *S. turris* cell, stained with FM4-64, during
566 valve formation and exocytosis. (MP4 2237 kb)
567
568
569
570
571
572
573